ICAS 2021 SHANG HAI
International Council of the Aeronautical Sciences
32nd Congress of the International Council of the Aeronautical Sciences
September 6-10, 2021
Pudong Shangri-La, Shanghai, China

STABILIZATION OF SUPERSONIC BOUNDARY LAYERS IN THE PRESENCE OF FAVORABLE PRESSURE GRADIENT

Chuvakhov P.V.
Central Aerohydrodynamic Institute (TsAGI), 1 Zhukovskogo Str., Zhukovsky, 140180, Russia
Moscow Institute of Physics and Technology (MIPT), 9 Institutskiy per., Dolgoprudny, 141701, Russia

Abstract

Expansion of supersonic flows may lead to boundary layer stabilization or relaminarization. Recent computations revealed that a turbulent spot originated from a wave packet in a Mach 3 flat plate boundary layer do not disappear passing expansion corner of 10°. Considered below is a turbulent spot that originates in a Mach 6 flat plate boundary layer dominated by second mode disturbances of acoustic nature. The spot development, its spectral characteristics and contribution to viscous friction are analyzed.

Keywords: expansion corner, supersonic boundary layer, turbulent spots, direct numerical simulation, stability

1. Introduction

Laminar-turbulent transition is one of the key problems of fundamental fluid dynamics and applied aerodynamics of flight vehicles of new generation, such as green airplanes with natural and/or artificial laminarization, and supersonic airplanes with low sonic boom level. A low-level disturbance environment and smooth surface are inherit flight conditions for such vehicles. Under these conditions, boundary layer transition goes through the stages of receptivity to stochastic disturbances, stability of the excited boundary layer disturbances and their nonlinear breakdown, which result in sudden occurrence of turbulent spots. The spots develop downstream and eventually merge with each other producing a turbulent boundary layer [1], which is observed experimentally (see e.g. [2–6]). Turbulence results in increase of wall friction and heat transfer by several times compared to those in a corresponding laminar boundary layer.

Flow expansion can attenuate the boundary layer turbulence [7, 8]. Expansion corner flows are as often as compression ones, though the former have been paid smaller attention. A corresponding literature review was given in [9], where a Mach 6 boundary layer stability over expansion corners of $5°$ and $10°$ was investigated using linear stability theory and direct numerical simulation of wave packets of a small amplitude. It was shown that new modes did not appear near the corner despite boundary-layer expansion fan interaction. The stabilization effect was attributed to a sudden thickening of a boundary layer past an expansion corner, which led to a shift of dominating frequency of the second mode of the boundary layer. Thus, the wave packet that grew over the flat plate part attenuates downstream the corner. The direct numerical simulation proved widely the findings of linear stability theory.

Using direct numerical simulation, similar conclusions were drawn for the linear stage of disturbance evolution in the case of Mach number 3, where the dominating wave was the first unstable boundary layer mode with oblique wave fronts [10]. Consideration of nonlinear disturbances revealed a temporary stabilization effect on a turbulent spot, that was to delay the development of the spot over the expansion corner. The spot went on developing downstream the corner.

By the present paper, we add consideration of nonlinear regime to the findings of [9] dealing with the development of turbulent spots over the expansion corners of $5°$ and $10°$ at Mach 6.

2. Numerical problem formulation

2.1 Numerical method

The Navier–Stokes equations are solved using the in-house solver, which implements an implicit finite-volume shock-capturing method with second-order approximation in space and time.

A Godunov-type total-variation-diminishing scheme with a Roe approximate Riemann solver is used. Reconstruction of the dependent variables at grid cell boundaries is performed using a third-order WENO (weighted essentially non-oscillatory) scheme. Newton and generalized minimal residual methods are used to solve an algebraic system of equations that approximates the partial differential equations. Despite the dissipative nature of the TVD scheme, it is feasible to simulate unstable disturbances in supersonic boundary layers using sufficiently fine computational grids (e.g. [11]). In particular, nonlinear oblique breakdown of a wave train at Mach 3 [12] agrees well with the results of [13] that were obtained using a high-order numerical method.

Present computations were carried out on high-performance multiprocessor computer clusters using a parallel version of the code. The MPI technology and PETSc library of linear algebra routines were employed. Initially structured grids were split up into multiple zones with node-to-node interzone connectivity. More details on the solver can be found in [14].

2.2 Problem specification

Consider a laminar flow past an expansion corner (sharp flat plate plus inclined plate) in a supersonic free stream of speed U_∞^*, density ρ_∞^* and temperature T_∞^*. Hereafter asterisks denote dimensional quantities and '∞' marks free-stream quantities. The governing equations are solved in a nondimensional form relative to the corresponding free-stream values, while pressure $p = p^*/(\rho_\infty^* U_\infty^{*2})$. The characteristic length scale L^* is 7.5 times less than the distance from the leading edge to the corner. The free stream Mach number is 6, the Reynolds number is $Re_{\infty.L} = \rho_\infty^* U_\infty^* L^*/\mu_\infty^* = 10^6$, freestream temperature $T_\infty^* = 73.2\ K$. The dynamic coefficient of viscosity μ is calculated using Sutherland's formula

$$\mu \equiv \frac{\mu^*}{\mu_\infty^*} = \frac{T_\infty + T_S^*}{T_\infty^* + T^*}\left(\frac{T^*}{T_\infty^*}\right)^{1.5} \equiv \frac{1+T_S}{1+T}\,T^{1.5},$$

where $T_S^* = 110.4\ K$. Specific heats ratio and Prandtl number are constants: $\gamma = 1.4, Pr = 0.72$.

Consider a three-dimensional computational domain of Cartesian topology. Its bottom face corresponds to the wall of the expansion corner. The wall is no-slip and isothermal: $(u, v, w) = \vec{0}$, $T_w = 150K/T_\infty^* \approx 2.05$. The basic flow comes through the left and top faces ('inlet'), and leaves the domain through the right face ('outlet'). The dependent variables are fixed at the inlet and are linearly extrapolated out of the domain at the outlet. The flow is symmetric in the spanwise (z) direction.

The following configurations are considered: flat plate at $\varepsilon = 0°$ (case FP), expansion angles of $\varepsilon = 5°$ (case EC05) and $\varepsilon = 10°$ (case EC10). The corner station is located at $x = l = 0$, where l is the wall-related coordinate ($x = l$ for $x < 0$, $x = l\cos\varepsilon$ for $x \geq 0$).

The computational procedure is multistage (see [9] for details). Turbulent spot evolution is computed in a subdomain that lays entirely under the bow shock wave due to viscous interaction near the plate leading edge. To guaranty that an initial turbulent spot is identical for all the three configurations (FP, EC05, EC10), a single spot is computed over the flat plate part at $x \in [-4.5;\ 0.2]$ until it comes up to the station $x = 0$ at $t = 4.3$. This x-interval is similar for all three cases. To this end, a steady state solution is perturbed at $t = 0$ using vertical blow-suction through a square hole on the wall surface $x \in [x_s, x_e] = [-4.1751, -4.0841]$, $z \in [z_s, z_e] = [-0.02275, 0.02275]$, with the mass flow rate distribution being

$$(\rho v)' = A\cos^3\left(\pi\frac{x - 0.5(x_e + x_s)}{x_e - x_s}\right)\cos^3\left(\pi\frac{z - 0.5(z_e + z_s)}{z_e - z_s}\right)(\sin(0.5\omega_0 t) + \sin(\omega_0 t)).$$

Here $\omega_0 = 62.5$ is the basic circular frequency, while the amplitude is large enough, $A = 5 \times 10^{-2}$, to produce a wave packet that evolves into the turbulent spot ahead of the corner station $l = 0$. Perturbation lasts for the time interval $2\pi/\omega_0$, which provides nearly flat frequency spectrum of the actuator over $\omega < \omega_0$. Numerical grid is excessively fine at this stage, $N_x \times N_y \times N_z = 4554 \times 233 \times 101$, which provides about 90 grid points per dominating wave length of the basic harmonic.

The resulting turbulent spot is then transferred to the domain extended downstream in x and z ($z \in [0; 0.3]$, $-2.2 \leq l \leq 6$, $y \in [0; 0.066]$), with upstream disturbance-free region removed ($l < -2.2$). The transfer is to add disturbance field to the mean flow using three-dimensional linear interpolation onto

the grid $N_x \times N_y \times N_z = 4201 \times 233 \times 151$ that provides about 47 grid points per the dominating wavelength in the streamwise direction. The wall normal resolution of the grid is 100–120 points across the boundary layer. It remains nearly same in the all cases considered. Note that transfer of disturbances from one grid to the other does not introduce any spurious perturbations to the solution. The computations proceed until the turbulent spot leaves the computational domain, i.e. residual becomes less than the target value of 10^{-4} over the entire flow field ($t_{max} = 20$). Finally, the wall pressure disturbance field $p'_w(t, l, z)$ is extracted by subtracting the undisturbed solution from the disturbed one and then analyzed.

The steady state flow field in the extended computational domain are shown in Fig. 1 for case EC10. A subdomain to simulate the turbulent spot evolution is marked by the white bold line at which the steady flow is fixed. Details on the steady-state solutions and advanced description of numerical problem formulation can be found in [9].

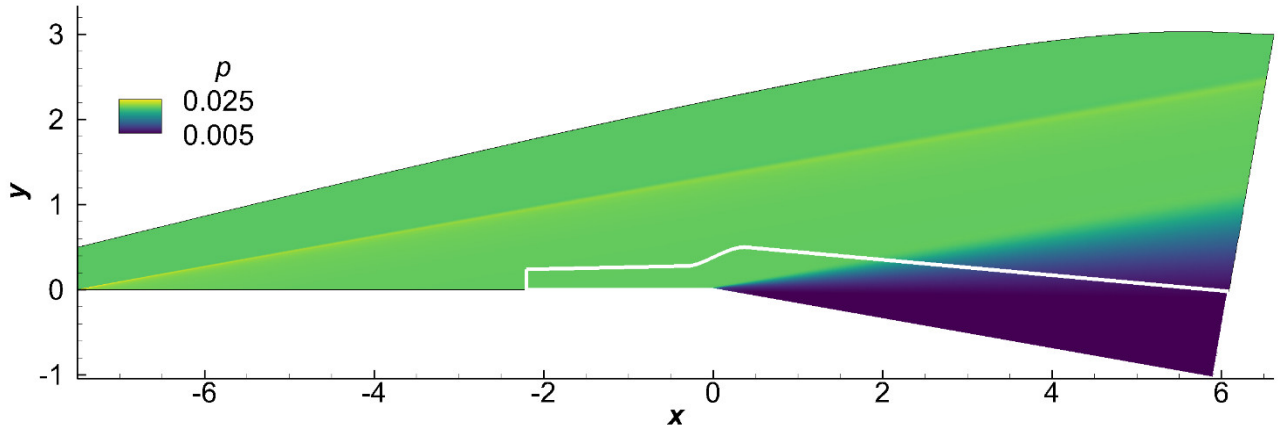

Figure 1 – Overall steady state pressure field and a computational subdomain (white line). Initial turbulent spot is located at $-2.2 < x < 0$ at $t = 4.3$.

2.3 Computing and analyzing results

Having been imposed by the blow-suction actuator, disturbances evolve downstream. The pressure disturbance field $p'_w(t, l, z)$ is collected at every l-station for the whole time interval $t \in [0; 20]$ during which the turbulent spot develops over the expansion corners. The collected $N_t \cdot N_l \cdot N_z$ values occupy a three-dimensional grid. First, fields of p'_w are considered along with the corresponding isosurfaces of Q-criterion. Next, p'_w is analyzed using two-dimensional Fourier transform in time t and spanwise coordinate z, at all l-stations.

3. Results

3.1 Disturbance evolution

Development of initial perturbation into the turbulent spot is illustrated in fig. 2. After being introduced, the disturbance forms a packet of flat waves with regular vertical fronts that corresponds to the second mode of the boundary layer at Mach 6. Next, a quick nonlinear breakdown stage is observed at which the packet deforms and finally turns into a young turbulent spot before the disturbance reaches the station $x = l = 0$. At $t = 4.3$ the turbulent spot is set off at one of the three wall configurations: FP, EC05, EC10. Figure 2 shows only the cases FP and EC10, while the results for EC05 are in-between.

No expansion corner influence is visible upstream the corner station. Passing above the corner, the spot pressure footprint becomes weaker, though the spot does not disappear downstream. Small vortical structures of the footprint are no longer observed when EC10 spot leaves the corner neighborhood compared with FP case. EC10 spot remains developing, while its expansion-related weakening remains uncompensated downstream: FP spot looks considerably stronger than that of EC10.

However, the spatial structure of EC10 turbulent spot does not appear to attenuate strongly, as illustrated in fig. 3 by isosurfaces of Q-criterion. The vortex structure remains well-developed and lifts away from the wall behind the corner. When EC10 spot overcomes the expansion, it proceeds growing along the inclined surface as if no expansion took place. Nevertheless, its dimensions are reduced compared to those of FP case. This observation points to the fact that the expansion introduces a delay into the development of a turbulent spot.

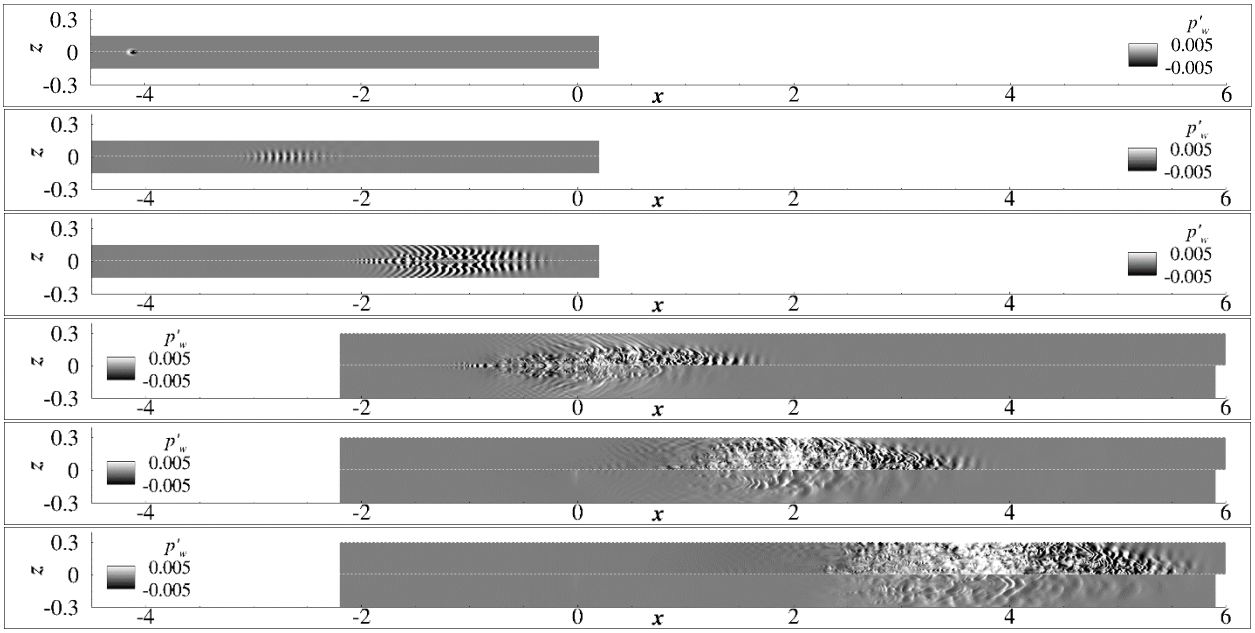

Figure 2 – Evolution of the turbulent spot by distribution of wall pressure disturbance at different time instants $t = 0.1, 2.15, 4.3, 6.45, 8.6, 10.75$ (top to bottom):
FP (upper subpanel of each panel); EC10 (lower subpanel of each panel).

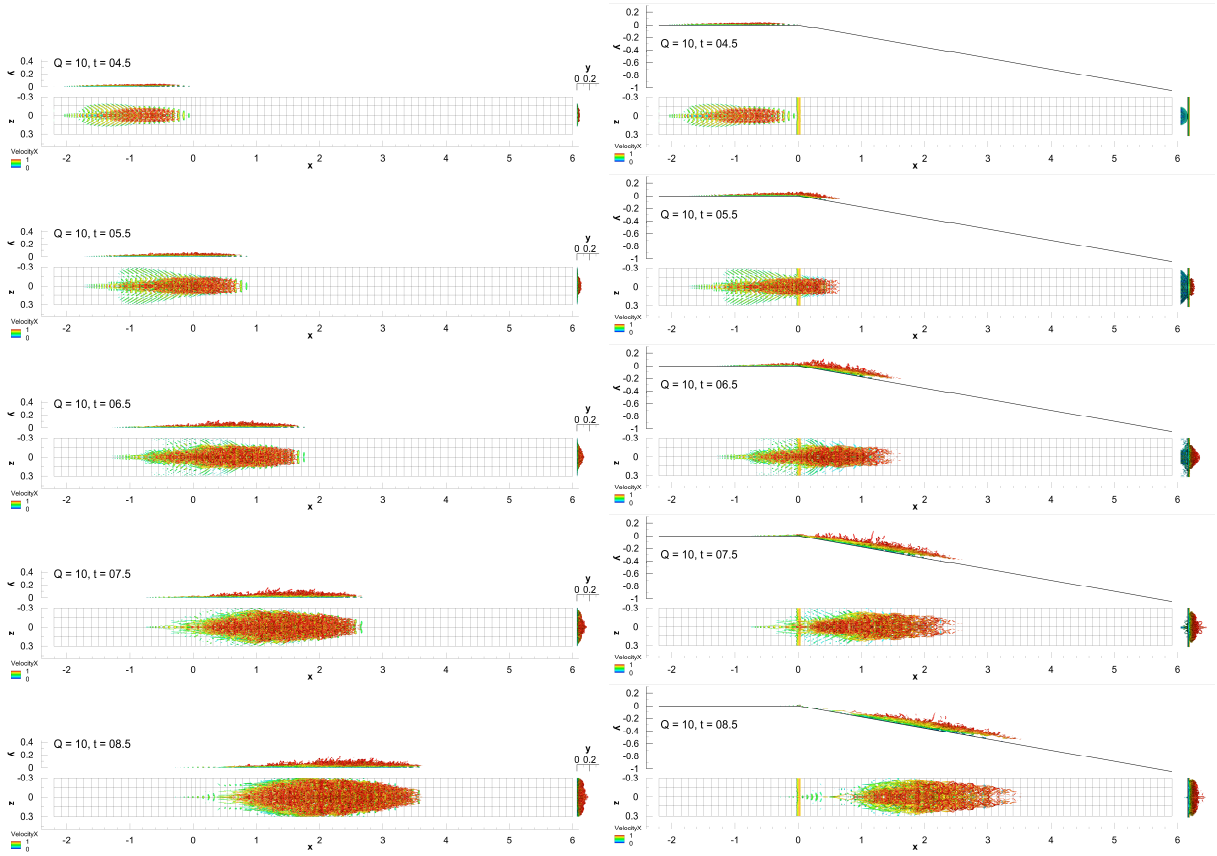

Figure 3 – Evolution of the turbulent spot by three projections of isosurfaces of Q-criterion at different time instants; FP (on the left); EC10 (on the right).

3.2 Disturbance spectra

The wall pressure disturbance spectra at several l stations are given in fig. 4.

As demonstrated in fig. 2 at $t = 2.15$, the early flat plat boundary layer disturbance looks like a regular second mode wave packet. This is supported by the spectrum at $l = -0.3$ (fig. 4a). It consists from a single maximum near $(\omega, \beta) \approx (90, 0)$ that corresponds to a flat wave that dominates the boundary layer. Close downstream the dominating wave shifts down in frequency in accord with linear stability theory, and multiple harmonics appear due to strong nonlinear interaction (fig. 4b, $l = -2$). So far, the spectrum has become wider in β, with few oblique ($\beta \neq 0, \omega \neq 0$) harmonics being born at the dominating frequency. This breakdown process resembles fundamental resonance mechanism when two oblique waves of a certain wave number amplify quickly at some frequency accompanied by the strong dominating wave at the same frequency. Nonlinear breakdown goes fast, and the disturbance demonstrates the behavior of a turbulent spot ahead of the corner, as illustrated for $l = -0.5$ in fig. 4c.

Downstream the corner, FP spot spectrum becomes distributed more evenly over the low-frequency band (fig. 4d-e). A zero frequency harmonic develops, which indicates that the mean flow has changed. The EC10 spectrum (fig. 4d) demonstrates that the spot is damped immediately at the corner over the whole Fourier space. The higher the frequency or wave number, the stronger the damping. Similar qualitative behavior is observed downstream (fig. 4e, f): low-frequency range harmonics are slowly recovered, though higher-frequency/wave number ones do not seem to recover their amplitudes at all.

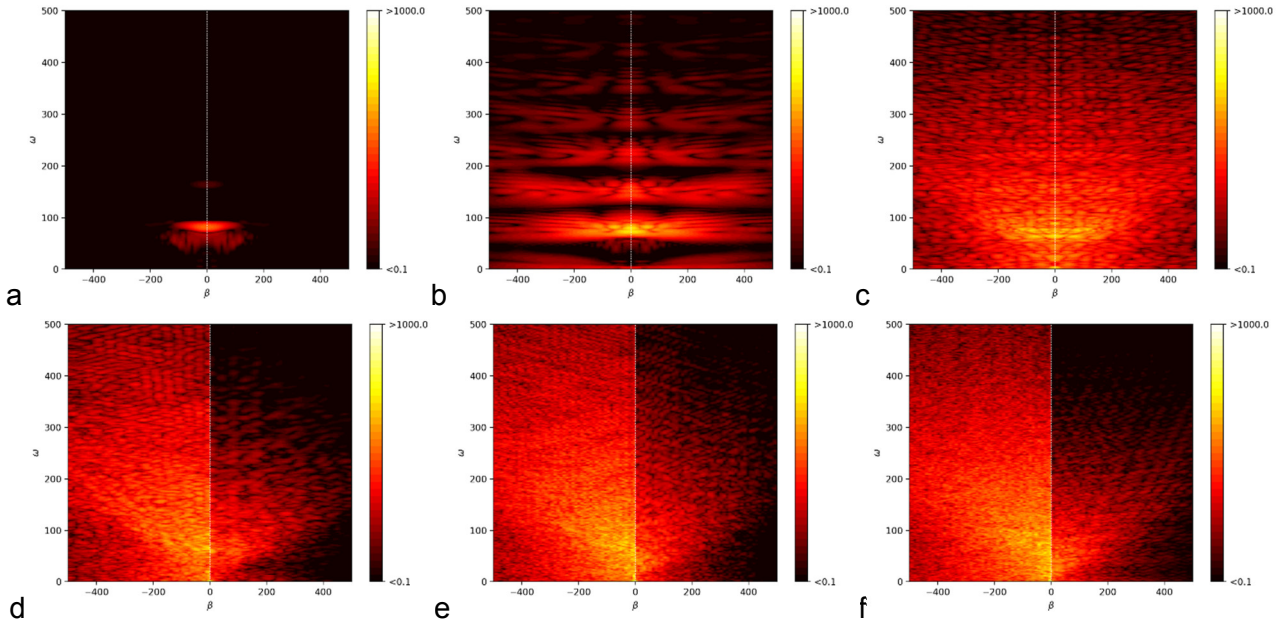

Figure 4 – Energy spectrum of the turbulent spot using two-dimensional Fourier transform at the stations l =-3(a), -2(b), -0.5(c), 0.5(d), 2(e), 3(f):
FP (left subpanel of each panel); EC10 (right subpanel of each panel).

The observed behavior of disturbance spectra supports the idea that turbulent spots do not disappear and proceed with developing downstream the corner with small scale components damped. It is also supported by the distribution of spanwise-maximum wall pressure disturbances as illustrated in fig. 5 (left) at few instants of time. In the all cases, the disturbance amplitudes evolve side by side up to the corner station, and becomes smaller just behind the corner for EC05 and EC10 configurations. Next downstream the amplitudes again are close, the larger the expansion angle, the lower the amplitude.

Distribution of the maximum spectral component amplitude supports that statement, as illustrated in fig. 5 on the right. They again keep tightly to each other for $l < 0$ and separate quickly at $l \approx 0$, while keep tracking each other downstream at $l > 0$. The less the value of expansion angle, the less the damping effect at the corner. The behavior of turbulent spots is quite different from that of linear wave packets [9], as compared in fig. 5 (right). The post-expansion boundary layer turns stable to

the wave packets developed upstream the corner, and the packets attenuate monotonically downstream (linear regime [9]). New post-expansion instabilities originate at low initial amplitudes. Thus, new amplifying wave packets get stronger much further downstream of the expansion. The overall effect of the expansion corner at linear regime resembles boundary layer stabilization.

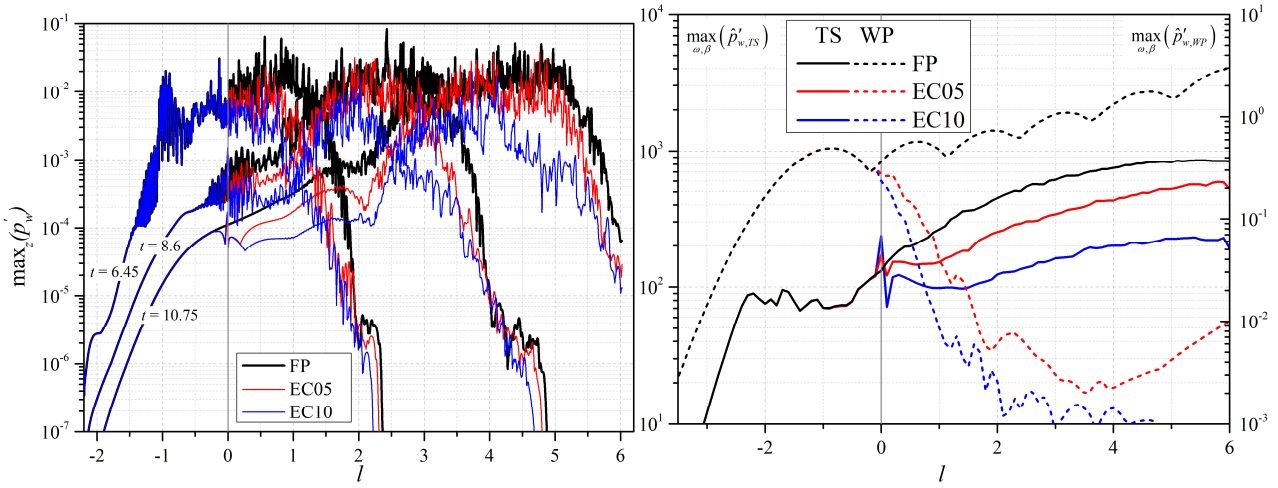

Figure 5 – Left: Distribution of spanwise-maximum wall pressure disturbance at three time instants: $t = 6.45, 8.6, 10.75$. Right: maximum Fourier amplitude over the entire set of harmonics. Linear wave packet (WP [9]) and nonlinear turbulent spot (TS) cases are compared.

3.3 Delay of turbulent spot

Given below is a try to estimate the delay effect of the flow expansion on the turbulent spot based on the spot's contribution to the force of viscous friction, $\Delta F_{v,x}$

$$\Delta F_{v,x} \approx \iint_S \Delta c_{f,x} dl dz,$$

where S is the surface area under the flow, while $\Delta c_{f,x}$ is the increase in local friction coefficient with respect to the case of laminar boundary layer. Friction coefficient is defined in a standard manner:

$$c_{f,x} = \frac{2\tau^*_{w,x}}{\rho^*_\infty U^{*2}_\infty} \equiv 2\frac{\mu_w}{Re_{\infty,L}}\left(\frac{\partial V}{\partial \vec{n}}\right)_{w,x},$$

where $\partial V/\partial \vec{n}$ is the derivative of velocity modulus along the wall normal direction. The station l_c where the additional force $\Delta F_{v,x}$ is applied is further referred to as the force center. It can be determined similar to definition of mass center of a body based on the problem geometry:

$$l_c = \iint_S l \cdot \frac{dF_{v,x}}{\Delta F_{v,x}}.$$

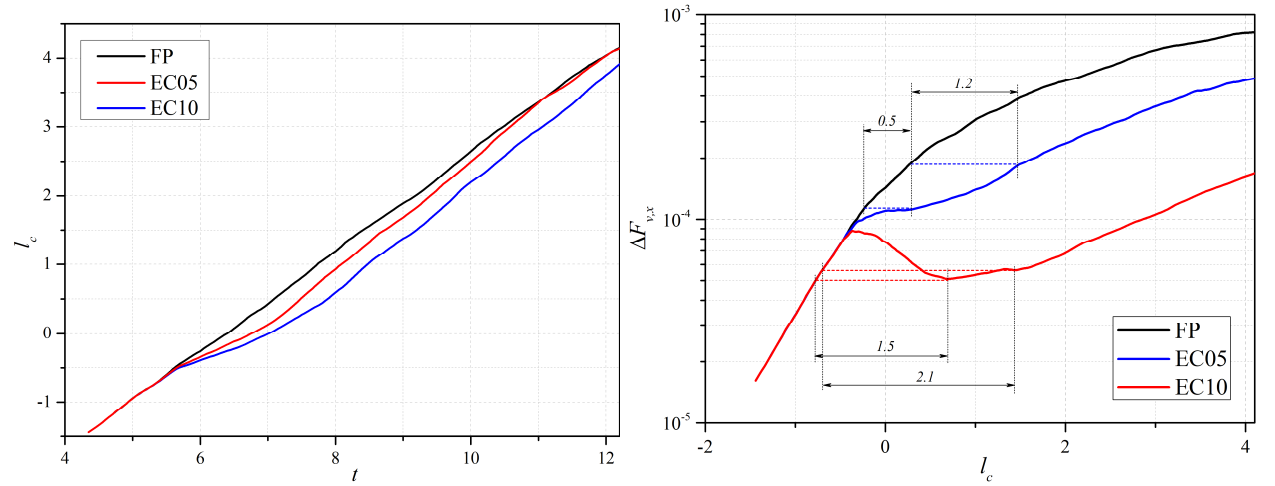

Figure 6 – Evolution of the application location of $\Delta F_{v,x}$ (left) and contribution of the turbulent spot to the friction force with dimensions are the possible estimation of a delay length (right).

First, consider propagation of the force centers $l_c(t)$ as illustrated in fig. 6 on the left. The centers moves together for $t < 5.5$, which corresponds to the spots located entirely ahead of the corner station. Upon overcoming the corner, the spots lose their strength as shown above. Therefore, the spot tail has an increasing share in $\Delta F_{v,x}$ as the spot starts passing the corner. This leads to decelerating of the force center, which is manifested as lower inclination of $l_c(t)$ in fig. 6 (left). The deceleration is observed until the tail becomes too small compared to the spot head to make a significant contribution to friction. Next, a reversed trend is expected, when the head resumes growing, while the tail is more and more suppressed by the expansion. Thus, the force center should first go slower and then faster as the spot fall over the corner. This is observed in fig. 6 (left) especially in the case EC05 and less pronounced for in the case EC10. Eventually, one would expect inclination to recover to some stationary value that should depend on the edge conditions of the boundary layer. It is known from numerical simulations, that turbulent spots have a nearly triangular shape. Its leading edge moves at speeds close to that at the boundary layer edge U_e, while its trailing edge moves at speeds about $0.5U_e$. Thus one would expect that the spots speed should be proportional to U_e that differs marginally for all the cases under consideration, as shown in [9]. Therefore, FP, EC05 and EC10 spots should have similar inclination of $l_c(t)$ far downstream of the expansion. Spots speed may be estimated by linear regression of $l_c(t)$ over the time interval $[8,12]$ as follows: FP – 0.723 ± 0.004, EC05 – 0.792 ± 0.005, EC10 – 0.786 ± 0.004; the uncertainty intervals are the doubled standard deviations of corresponding linear regression procedure.

Consider evolution of the contribution of the turbulent spots to viscous friction, $\Delta F_{v,x}$ (fig. 6, on the right). The force center lays inside the spot, so the value of l_c is negative as the spot starts passing the corner. It quickly turns positive on the contrast to the case of Mach number 3 discussed in [10]. This might be related to elongation of the turbulent spots at higher Mach numbers. Downstream the corner, the spot contribution rate decreases (EC05) or ever becomes negative (EC10) attaining its minimum. Eventually, the spot contribution continues increasing at the rates proportional to those for FP case. The overall effect of the corner on the turbulent spot can be expressed using a length of delay Δl, at which the corner decelerating effect is present and growth rate of the contribution $\Delta F_{v,x}$ is reduced relative to the corresponding FP value, as illustrated in fig. 6 (right). The delay lengths can be estimated in different ways depending on the criterion. If one adopts the proportionality of EC and FP cases, the lengths are about 1.2 and 2.1 for cases EC05 and EC10, respectively. Alternatively, if one adopt monotonical growth of $\Delta F_{v,x}(l)$, the length would be 0.5 (EC05) and 1.5 (EC10), as illustrated in fig. 6 on the right. Generally, this length should illustrate the station where a turbulent spot resumes its development as if it did not lose in $\Delta F_{v.x}$ due to flow expansion.

It is to be emphasized that the turbulence contribution to friction is not related with a single turbulent spot by the end of the computational domain. It should rather be considered as the effect of merging spots because the disturbances come close to symmetry boundary at $z = z_{max}$. This fact should manifest itself as a slower growth of $\Delta F_{v.x}$ with l.

4. Conclusion

Numerical simulation a turbulent spot in supersonic expansion corner boundary layers at Mach number 6 is carried out. Expansion angle is varied among $0°$ (flat plate case), $5°$, $10°$. Turbulent spots are weakened near the corner and continue their growth away downstream the expansion as if their development was delayed for a certain length. The weakening effect increases with the expansion angle.

Distribution of wall pressure disturbance and spot contribution to viscous friction showed that the wall-observed effects due to flow expansion can be treated as boundary layer laminarization while the turbulence does not die and may return into the boundary layer downstream.

5. Acknowledgements

The work has been carried out in Central Aerohydrodynamic Institute under the support of Russian Foundation for Basic Research (Project no. 18-38-20091) using computing resources of the federal collective usage center Complex for Simulation and Data Processing for Mega-science Facilities at NRC “Kurchatov Institute”, http://ckp.nrcki.ru/.

6. Contact Author Email Address

mailto: pavel_chuvahov@mail.ru

7. Copyright Statement

8. References

[1] Emmons HW. The laminar-turbulent transition in a boundary layer-part I. *J. Aerosp. Sci.*, Vol. 18, pp 490–498, 1951.

[2] Jewell JS, Leyva IA and Shepherd JE. Turbulent spots in hypervelocity flow. *Exp Fluids*, Vol. 58, No. 4, 2017.

[3] Srichan S, Rakpakdee W, Kiatsiriroat T and Chaiworapuek W. Thermal characterization of longitudinal merging of turbulent spots. *Experimental Heat Transfer*, Vol. 32, No. 5, pp 1–21, 2018.

[4] Casper KM, Beresh SJ, and Schneider SP. A preliminary study of the longitudinal merging of instability wave packets and turbulent spots in a hypersonic boundary layer. *42nd AIAA Fluid Dynamics Conf. Exhibit*, NewOrleans, LA, USA, pp. 1–15., 25–28 June 2012.

[5] Casper KM, Beresh SJ and Schneider SP. Pressure fluctuations beneath instability wavepackets and turbulent spots in a hypersonic boundary layer. *J Fluid Mech,* Vol. 756:1058–91, 2014.

[6] Fiala A, Hillier R, Mallinson SG and Wijesinghe HS. Heat transfer measurement of turbulent spots in a hypersonic blunt-body boundary layer. *J Fluid Mech*. Vol.555, 2006.

[7] Gol'dfel'd MA., Zinov'iev VN. and Lebiga VA. Structure and Fluctuation Characteristics of a Compressible Turbulent Boundary Layer Behind a Fan of Rarefaction Waves. *Fluid Dynamics*, Vol. 22, No. 1, pp. 40–45, 1987.

[8] Goldfeld MA, Nestoulia RV. and Shiplyuk AN. Relaminarization of Turbulent Boundary Layer with a Mach Number M_∞=4. *Journal of Applied Mechanics and Technical Physics*, Vol. 43, No. 1, pp. 76–82, 2002.

[9] Chuvakhov PV, Egorov IV, Ilyukhin IM, Obraz AO and Fedorov AV. Boundary-Layer Instabilities in Supersonic Expansion Corner Flows. *AIAA Journal*, 2021, available online: https://doi.org/10.2514/1.J060145

[10] Chuakhov PV and Egorov IV. Numerical simulation of disturbance evolution in the supersonic boundary layer over an expansion corner. *Fluid dynamics*, to be published in no. 5; 12 P, 2021, DOI: 10.31857/S0568528121050029

[11] Chuvakhov PV, Fedorov AV and Obraz AO. Numerical simulation of turbulent spots generated by unstable wave packets in a hypersonic boundary layer. *Computers & Fluids*, Vol. 162, pp. 26–38, 2018.

[12] Egorov I, Nguyen N, Nguyen T, Chuvakhov P. Simulation of laminar-turbulent transition using dissipative numerical schemes. Computational Mathematics and Mathematical Physics, Vol. 61, pp.254-266, 2021.

[13] Christian SJ. von Terzi MDA and Fasel HF. DNS of Complete Transition to Turbulence via Oblique Breakdown at Mach 3. AIAA paper 2008-4398, 2008.

[14] Egorov IV and Novikov AV. Direct numerical simulation of boundary layer flow over a flat plate at hypersonic flow speeds. Comput. Math. Math. Phys., Vol. 56 (6), pp. 1048–1064, 2016.